



Analytical Modelling of a Six-Phase Surface Mounted Permanent Magnet Synchronous Motor

T. Truong Cong^a, T. Nguyen Vu^{a,b}, D. Bui Minh^{a,b}, H. Vo Thanh^c, V. Dang Quoc^{*a,b}

^a *Laboratory of High-performance Electric Machines (HiPems), Viet Nam*

^b *School of Electrical and Electronic Engineering, Ha Noi University of Science and Technology, Viet Nam*

^c *Faculty of Electrical and Electronic Engineering, University of Transport and Communications, Ha Noi, Viet Nam*

PAPER INFO

Paper history:

Received 21 November 2023

Received in revised form 24 December 2023

Accepted 06 January 2024

Keywords:

Multiple Phase Surface Permanent Magnet Synchronous Motor

Back Electromotive Force

Cogging Torque

Torque Ripple

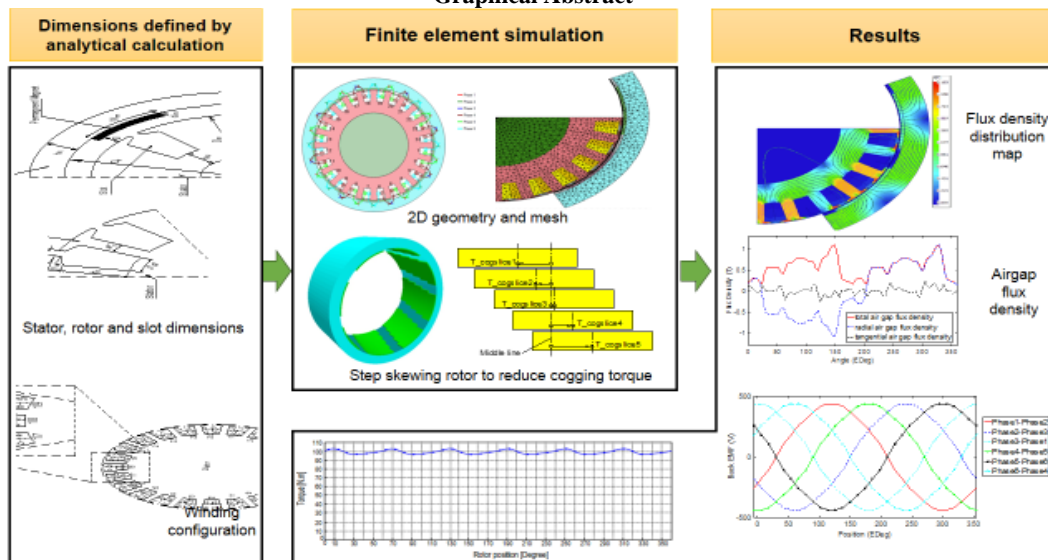
Analytical Model

ABSTRACT

A multi-phase permanent magnet synchronous motors (PMSM) has applied popularly in the field of industry (e.g. trucks, ship propulsion, mining, etc) due to its high torque, efficiency and reliable operation. So far, many researchers have studied the multi-phase PMSM (e.g. a three-phase PMSM, a six-phase PMSM) for electric vehicle applications. But, there are still significant limitations in the quantity of research on the six-phase PMSMs. Particularly, when researching this type of motor, authors mainly have provided specifications of the six-phase PMSMs and then conducted experiments on these machines without giving the detailed formulations to analytically compute and design dimensions and electromagnetic parameters. In this research, an analytic model is first developed to determine the main parameters of a six-phase surface-mounted PMSM (SPMSM). The finite element method (FEM) is then introduced to simulate and compute electromagnetic parameters, such as the current waveform, back electromotive force (EMF), flux density distribution, output torque, cogging torque, torque ripple and harmonic components. The development of proposed methods is applied on a practical problem of a six-phase SPMSM of 7.5kW.

doi: 10.5829/ije.2024.37.07a.07

Graphical Abstract



*Corresponding Author Email: vuong.dangquoc@hust.edu.vn (V. Dang Quoc)

Please cite this article as: Truong Cong T, Nguyen Vu T, Bui Minh D, Vo Thanh H, Dang Quoc V. Analytical Modelling of a Six-Phase Surface Mounted Permanent Magnet Synchronous Motor. International Journal of Engineering, Transactions A: Basics. 2024;37(07):1274-83.

1. INTRODUCTION

A six-phase permanent magnet synchronous motor (PMSM) has been recently used widely for electric vehicle applications. Because these motors have the high torque, power density, efficiency, wide speed range, reliability, durability and safety (1-5). Therefore, their extensive applications have been applied popularly in the fields of industrial, medical, aerospace and military sectors. Specifically, they are used in applications of electric vehicles, electric tractions, collaborative robots, drones electrical drive systems. So far, many researchers, designers and manufacturers have also studied three phase PMSMs. However, compared to the six phase PMSMs, these motors are still limitations for the torque and efficiency (6). In order to improve the performance and reliability of these machines, a six-phase PMSM has been proposed to use in applications demanding the high torque, efficiency and reliability. A novel configuration for a six-phase direct-drive PMSM called the 60° phase-belt toroidal winding configuration (60° -TW) was presented (1) via the finite element method (FEM) to compute the magnetic field distribution, back electromotive force (EMF), cogging torque, output torque and efficiency. In this paper, unlike conventional methods, each coil in the 60° -TW was here wound in the same direction on the stator yoke. Patel et al. (2), proposed a novel winding arrangement for the six-phase PMSM featuring 18 slots and 8 poles. This innovative configuration served to eliminate undesirable space harmonics within the stator magnetomotive force (MMF). Consequently, it leads to enhancements in power/torque density and efficiency while concurrently reducing eddy current losses in the rotor PMs and copper losses in the end windings. In addition, to improve the availability of the drive train for electric vehicles (EV) applications, this paper presented the concept of designing a six-phase PMSM as two distinct three-phase windings. A comprehensive investigation was carried out to explore various possible phase shifts between these two sets of three-phase windings, accounting for their slot-pole combinations and winding arrangements. The optimal phase shift was then selected through an analysis of harmonic distributions and their impact on the machine performance. Scuiller et al. (3) introduced a design approach tailored for multi-phase PMSMs powered by pulse-width modulation (PWM) voltage source inverters. Initially, the potential for enhancing the torque density through harmonic utilization is presented. Then, the distinctive challenges stemming from the PWM-based power supply of multi-phase machines in the design process are addressed. Islam et al. (4) conducted a performance comparison of a five-phase external rotor PM assisted synchronous reluctance motor with two distinct winding configurations. In this context, a five-phase winding configuration proposed

enhancements in power density, fault tolerance capabilities and the mitigation of torque pulsations, in contrast to conventional three-phase windings. Additionally, the incorporation of an external rotor structure contributes to further increases in power density. In, a novel six-phase PMSM with an innovative toroidal winding (NTW) configuration was also presented by Jin et al. (5) to investigate electromagnetic parameters such as the back EMF, cogging torque, torque ripple, output torque, losses and magnetic field distribution. In this paper, each coil of the NTW is uniformly wound onto the stator yoke in the same direction. The obtained results enhanced the low-speed performance and increased the output torque. They were also compared to the traditional six-phase PMSM. Del Pizzo et al. (6) explored two potential electric propulsion motor solutions for unmanned aerial vehicles. It involves a comparison of the sizes, weights, and certain characteristics between a three-phase PMSM and a six-phase motor achieved through a suitable rewinding of the armature, while maintaining fixed stator and rotor magnetic circuits. Won et al. (7) presented an innovative electric truck application featuring a six-phase fractional-slot concentrated winding PMSM. This machine design comprised a dual three-phase winding, spaced 75 degrees apart. A mathematical model for the six-phase interior PMSM (IPMSM) using the -d and-q axis theory was conducted (8). This model was subsequently utilized to deduce the precise interrelationships among different unitized machine parameters, aiming to achieve optimal performance in both inverter control (IC) and traction scenarios. Cheng et al. (9) analyzed a modeling of a six-phase surface mounted PMSM (SPMSM) based on the equivalent magnetic circuit with the magnetic behavior and electrical characteristics.

Despite many papers have researched on six-phase PMSMs as discussed above. However, there are still significant limitations in the quantity of research on these machines. Particularly, when researching these types of motors, authors mainly have provided specifications of the six-phase PMSM and then conducted experiments on these motors without giving the detailed analytical formulations for computing and analyzing their electromagnetic parameters.

In this research, an analytical design is proposed for a six phase SPMSM to determine required dimensions and electromagnetic parameters as well. Then, the FEM is introduced to verify the analytical model via the simulation of the current waveform, back EMF, flux density distribution, output torque, cogging torque, torque ripple and harmonic components.

2. MODEL OF A SIX PHASE PMSM

A structure of the six-phase SPMSM with the 60° toroidal winding (TW) is depicted in Figure 1.

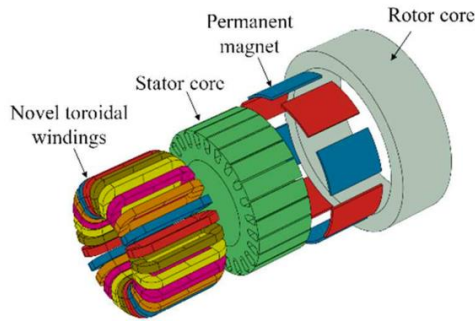


Figure 1. Modeling of the six-phase PMSM with 60°-TW (5)

This design consists of an outer rotor core, an inner stator core and the distinctive 60°-TW. Unlike the conventional winding approach, each coil is wound onto the stator yoke in the 60°-TW (5). The structural characteristics of the 60°-TW is illustrated in Figure 2. The arrangement of stator windings for the six-phase PMSM with 60°-TW is illustrated in Figure 3.

3. ANALYTICAL DESIGN

In this part, a six-phase outer rotor SPMSM of 7.5kW with a 60°-TW configuration is analytically designed. The input parameters of this machine are presented in Table 1.

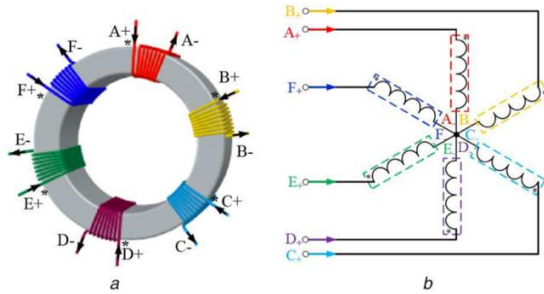


Figure 2. Structure of simplified stator of the six-phase PMSM with 60°-TW (5)

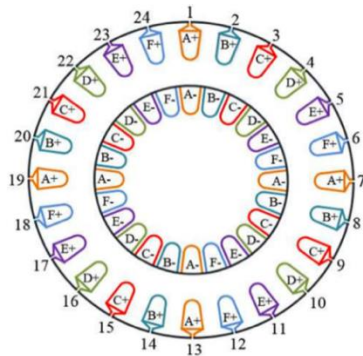


Figure 3. Arrangement of stator windings (5)

TABLE 1. Main parameters of outer rotor SPMSM

Parameters	Value	Unit
Continuous power	7.5	kW
Phase terminal voltage	200	V
Number of phases	6	phase
Number of slots	24	slot
Number of pole pair	4	pole pair
Rated torque	95.5	N.m

In a design process, the determination of parameters for PM is extremely an important part of the SPMSM as it produces the magnetic field in the air gap.

The strength of magnetic field due to the PM in the SPMSM consists of the width, length, thickness and the pole embrace. Figure 4 shows the demagnetization curves of polarization (J) and magnetic flux density (B), where the PM of NdFeB N38SH with the remanence of 1.26 T (at 20°C) and the normal working point of 0.9 T are used in this study. The main dimensions of the magnetic core are presented in Figure 5. The magnetic flux density in the air gap (B_g) is defined as:

$$B_g = \frac{4}{\pi} \sin(\alpha) B_m, \quad (1)$$

where α is the half coverage angle defined in electrical degree and B_m is the magnetic field density due to the PM. The PM thickness is defined then as:

$$d_m = \frac{\mu_m g_{eff}}{B_r A \sin(\alpha) - 1} B_g \pi \quad (2)$$

where μ_m , g_{eff} and B_r are respectively the permeability of PM, length of effective air gap and remanence of PM. The g_{eff} is defined via the air gap length (g) and Carter's factor (k_c), i.e (10),

$$g_{eff} = k_c \cdot g \quad (3)$$

for

$$k_c = \frac{\tau_s}{\tau_s - \gamma g} \quad (4)$$

where τ_s is the slot pitch and can be defined as:

$$\tau_s = \frac{\pi(D_{ir} - 2g)}{Z} \quad (5)$$

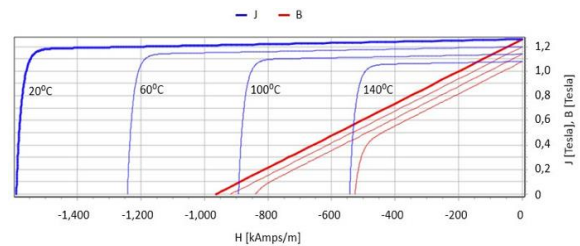


Figure 4. Demagnetization curves for N38SH (11)

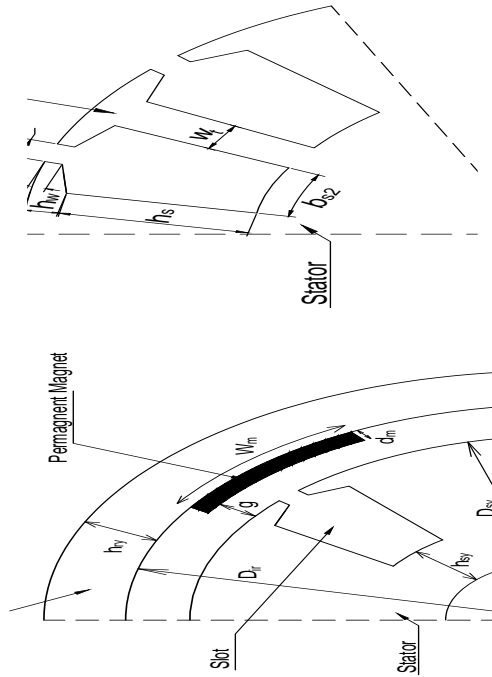


Figure 5. Main dimensions of the magnetic core (top) and slot (bottom)

where D_{ir} is the inner diameter of rotor and Z is the number of slots. The factor if PM motor (γ) is computed via the below expression (10):

$$\gamma = \frac{2b_s}{\pi g} \left[\arctan\left(\frac{b_{so}}{2(L+g)}\right) - \frac{L+g}{b_{so}} \ln \sqrt{1 + \left(\frac{b_{so}}{2(L+g)}\right)^2} \right] \quad (6)$$

where b_{so} is the width of slot opening and L is the length of PM, which is equal to the length of the both rotor and stator. The width of PM (w_m) can be now defined:

$$w_m = \frac{\alpha D_{ir}}{p} \quad (7)$$

where p is the number of pole pair. The volume of the armature part being an essential parameter in determining the D_{ir} and L can be calculated as (10):

$$\frac{\pi}{4} D_{ir}^2 L = \frac{M_n k_{safe}}{2\sigma_m} \quad (8)$$

where M_n is the rated torque of the motor, k_{safe} is the safe factor ($k_{safe} = 2 \div 3$), σ_m is the value of the shear stress of the PM (for material (NdFeB), it can be $\sigma_m = 20 - 50$ kPa). It should be noted that the relation between the D_{ir} and L is presented through the shaping coefficient (k_{shape}), that is:

$$k_{shape} = \frac{L}{D_{ir}} \quad (9)$$

From the Equation 9, the value of D_{ir} and L can be computed.

In addition, the height of stator yoke (h_{sy}) and rotor

yoke (h_{ry}) can be respectively determined as:

$$h_{sy} = \frac{B_m w_m}{2B_{sy}}, \quad h_{ry} = \frac{B_m w_m}{2B_{ry}} \quad (10a-b)$$

where the fields B_{sy} and B_{ry} are respectively the flux densities at the stator and rotor yokes given in Table 2. The width of tooth (w_t) is now defined:

$$w_t = \frac{2pB_m w_m}{ZB_t} \quad (11)$$

where B_t is the tooth flux density given in Table 2.

The number of conductors (N_c) per coil is given as:

$$N_c = \frac{U_{phase}}{2\pi\sqrt{2}f q k_w B_g \cos\delta D_{ir} L} \quad (12)$$

where U_{phase} , f , q , k_w and δ represent the phase voltage, frequency, number of slot per pole per phase, winding factor and torque angle, respectively. The torque angle for SPMSM is usually designed in the range of $15 \div 30$ degrees. In this study, it is chosen as 20 degrees (2). The slot area can be calculated as:

$$A_{slot} = \frac{4N_c A_{Cu}}{k_{fill}} \quad (13)$$

where A_{Cu} is the copper area of the conductor and k_{fill} is the slot filling factor.

As presented in Figure 5, the slot top width (b_{s1}), slot bottom width (b_{s2}), slot height (h_s) can be calculated as the below expressions:

$$b_{s1} = \frac{\pi(D_{os} - 2h_{so} - 2h_w)}{Z} - w_t \quad (14)$$

$$b_{s2} = \sqrt{\frac{b_1^2 - 4\pi \times A_{slot}}{Z}} \quad (15)$$

$$h_s = \frac{2A_{slot}}{b_1 + b_2} \quad (16)$$

where h_{so} and h_w are respectively the height and wedge of the slot opening.

Based on the analytical calculation process above, the required dimensions of a six-phase outer rotor SPMSM of 7.5 kW are given in Table 3.

4. ANALYSIS OF NO AND FULL LOAD OPERATIONS

In this part, the machine is operated under no-load conditions considered as a valuable means of assessing the motor magnetic circuit, a crucial element in motor

TABLE 2. Value of magnetic Densities of PM machine (5)

Position	Flux density (T)
Stator yoke	1.0 – 1.5
Rotor yoke	1.0 – 1.5
Tooth	1.6 – 2.0

TABLE 3. Main dimensions of a six-phase SPMSM of 7.5kW

Parameters	Value	Unit
D_{tr}	224	mm
L	112	mm
h_{ry}	19	mm
g	1	mm
w_m	63,53	mm
d_m	2,5	mm
w_t	10,6	mm
h_s	22,9	mm
b_{s1}	17	mm
b_{s2}	11	mm
b_{so}	5	mm
h_{so}	1	mm
h_w	2	mm
h_{sy}	19	mm
N_c	44	turn
n_c	224	

design. This paper focuses on studying the electromagnetic parameters such as the magnetic flux density distribution, back EMF, output torque, cogging torque and torque ripple. Based on the required parameters already given in Table 3, a 2-D model of the proposed motor is considered for both no and full load conditions.

The no-load back-EMF depending on several factors (such as winding factors, number of turns per phase, magnetic flux density in air gap, frequency) is defined as follows (2).

$$E_0 = \sqrt{2} \sin\left(\frac{y\pi}{\tau 2}\right) \frac{1}{q} \left| \sum_{m=1}^{N_c} e^{-j\theta_m} \right| p B N_c \tau f L \quad (17)$$

where y is the coil pitch, τ is the pole pitch, f is the frequency (Hz), q is the slot number of single phase per pole and θ_m is the electrical angle between adjacent slots. The term j is expressed as the current direction (with $i = 1$ for the positive current direction and $i = -1$ for the negative current direction).

The cogging torque is a type of torque appearing on the teeth that can lead to the vibration and noise in SPMSM (12, 13). When using the SPMSM in variable speed drive applications, if the frequency of torque fluctuations aligns with the mechanical resonance frequency of the stator or rotor, it can amplify the vibration and noise originating from the cogging torque. Thus, the calculation of the cogging torque is very importance in the design and production of high-performance SPMSMs.

The expression for the cogging torque (T_{cog}) is computed via the following equations (11, 14-17).

$$T_{cog}(\theta) = \frac{2LB_g^2 Z p}{\pi \mu_0 N_L} (R_{in}^2 - R_{out}^2) T_k \quad (18)$$

$$T_k = \sum_{k=1}^{\infty} \frac{K_{sk}}{k} \sin\left(k N_L \frac{b_0}{2}\right) \sin\left(k N_L \frac{\alpha_p}{2p}\right) \sin\left(k N_L \left(\theta - \frac{\alpha_s}{2}\right)\right) \quad (19)$$

$$K_{sk} = \frac{2 \sin\left(\frac{k N_L \alpha_s}{2}\right)}{k N_L \alpha_s} \quad (20)$$

where

- B_g is the maximum magnetic flux density in air gap,
- N_L is the lowest common multiple of N_s and $2p$,
- μ_0 is the permeability of air,
- R_{in} is the inner radius of the air gap,
- R_{out} is the outer radius of the air gap,
- b_0 is the slot opening,
- α_p indicates the pole-arc to pole-pitch ratio,
- α_s is the skewing angle,
- K_{sk} is the skew factor.

5. SIMULATION RESULTS

Based on the required dimensions obtained from the analytical model given in Table 3, the FEM is introduced to compute and analyse the electromagnetic parameters of the proposed motor. The first step is considered with no skewing PM to see the waveform of the back EMF, then a skewing PM technique is presented to improve this draw back.

The 2-D geometry and mesh are presented in Figures 6 and 7, respectively. Winding configurations of a six-phase outer rotor SPMSM is presented in Figure 8. The direction of currents in the six-phase winding is pointed out in Table 4.

The distribution of back EMF waveform and output torque of the six-phase outer rotor SPMSM are shown in Figures 9 and 10, respectively. It can be seen that in

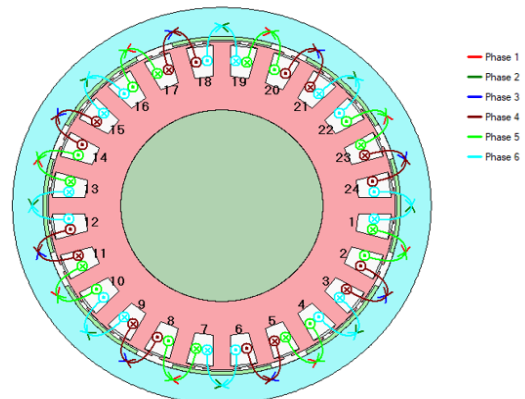


Figure 6. Geometry of the proposed motor in 2D

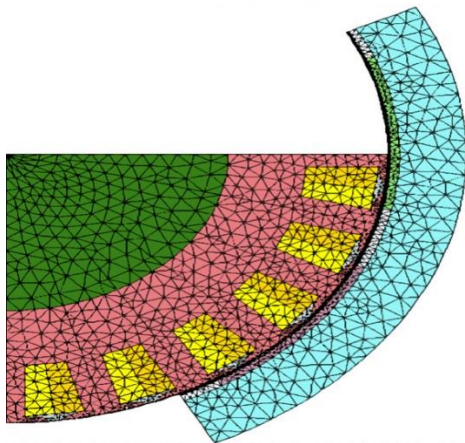


Figure 7. 2D-Mesh on a quarter view of model

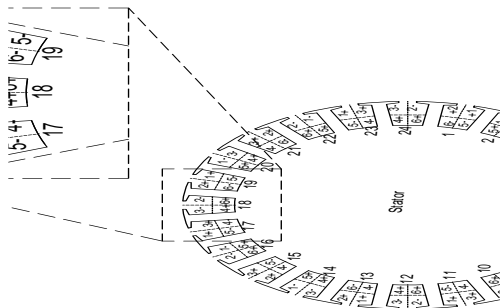


Figure 8. Winding configurations of a six-phase outer rotor SPMSM

TABLE 4. Direction of currents

Slots	Current directions	Slots	Current directions	Slots	Current directions
1	2+ 1+	2	1- 3-	3	3+ 2+
	6- 5-		5+ 4+		4- 6-
4	2- 1-	5	1+ 3+	6	3- 2-
	6+ 5+		5- 4-		4+ 6+
7	2+ 1+	8	1- 3-	9	3+ 2+
	6- 5-		5+ 4+		4- 6-
10	2- 1-	11	1+ 3+	12	3- 2-
	6+ 5+		5- 4-		4+ 6+
13	2+ 1+	14	1- 3-	15	3+ 2+
	6- 5-		5+ 4+		4- 6-
16	2- 1-	17	1+ 3+	18	3- 2-
	6+ 5+		5- 4-		4+ 6+
19	2+ 1+	20	1- 3-	21	3+ 2+
	6- 5-		5+ 4+		4- 6-
22	2- 1-	23	1+ 3+	24	3- 2-
	6+ 5+		5- 4-		4+ 6+



Figure 9. Back EMF waveform without using the skewing technique

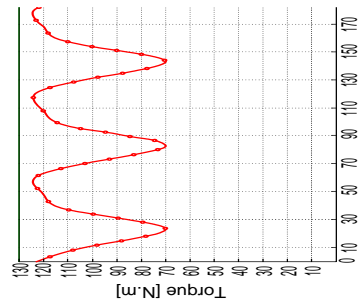


Figure 10. Output torque waveform without using the skewing technique

Figure 9, the waveform is still non sinusoidal due to high harmonic components. Thus, to make sure that the back EMF waveform is sinusoidal, the skewing technique for the PM with different angles is proposed as in Figure 11. Here, the PM is divided into five segments with different angles as given in Table 5. The minimal cogging torque with the use of skewing PM technique is presented in Figure 12. It should be noted that when the skew angle is chosen, the PM skew angle is zero for a symmetric case (see Table 5). These angles are chosen randomly to show how well the skewing technique could bring. However, these angles can be used in an optimization process to obtain the best result with the minimum torque ripple.

The map of flux density distribution with the skewing PM technique is shown in Figure 13. It can be seen that

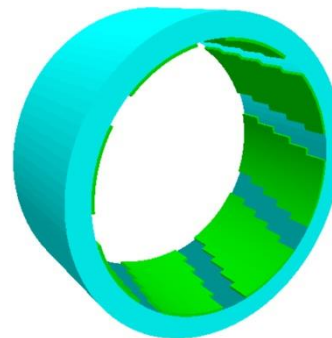


Figure 11. PM with the skewing technique

TABLE 5. Skewing angle of the PM with five slices

Segments	Angles
1	-6
2	-3
3	0
4	3
5	6

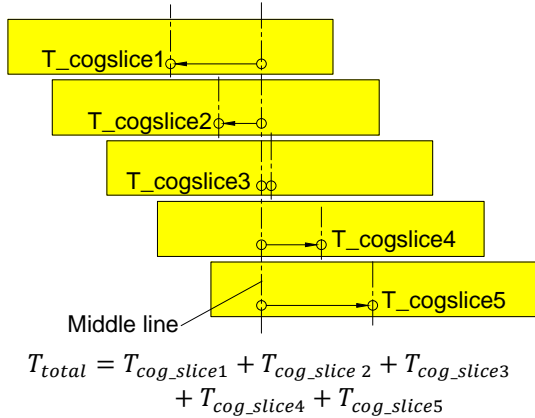


Figure 12. Cogging torque with skewing PM technique

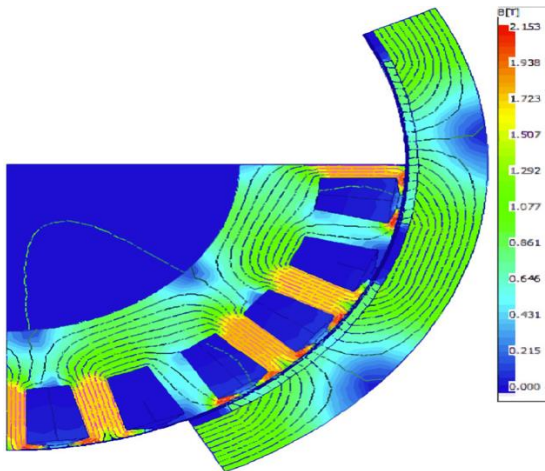


Figure 13. Flux density distribution with the skewing PM technique

the maximum value is 2.153 T, which is acceptable. It should be also noted that the higher value of flux density concentrates on the teeth and the corner of tooth tips due to the small area while the other parts of the core have the smaller value of flux density. The distribution of flux density waveform consisting of both the radial and tangential fluxes in the air gap is presented in Figure 14.

The harmonic components for this field is analyzed as shown in Figure 15. The flux linkage in no load and full load mode waveform and their harmonics order are also

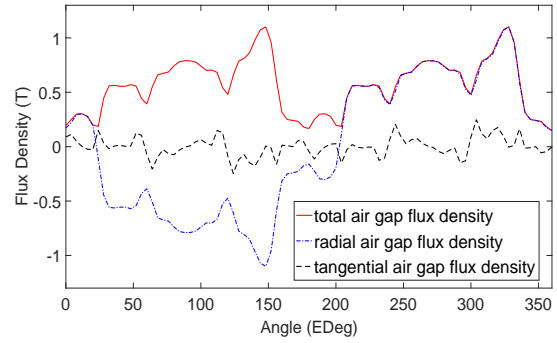


Figure 14. Waveform of air gap flux density

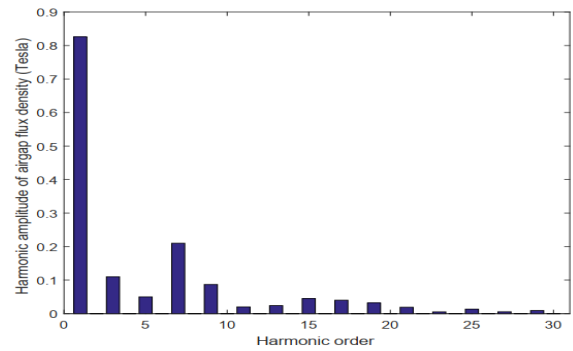


Figure 15. Harmonic components of the air gap flux density

presented in Figures 16 and 17. The back EMF waveform after using the skewing technique is shown in Figure 18. It can be seen that it is almost sinusoidal, which is the expected output result. The harmonic order of the line-line back EMF with the harmonic distortion of 2.785% is shown in Figure 19. The output torque waveform is pointed out in Figure 20. Its torque ripple is shown in Figure 21, with the value of under 3.5%.

The torque ripple holds significant importance in the design. One of the main reasons appearing the torque ripple is the cogging torque that is presented in Figure 22. This outcome signifies the motor's stable and smooth operation, a crucial aspect to be attained in the overall design.

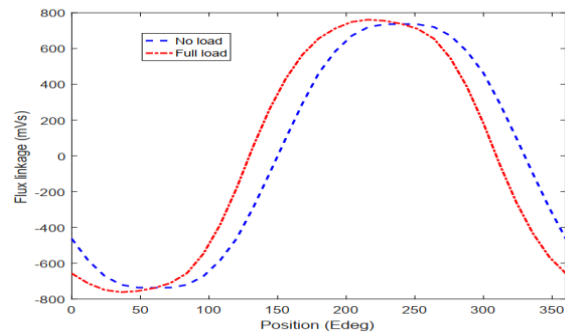


Figure 16. Flux linkage waveform

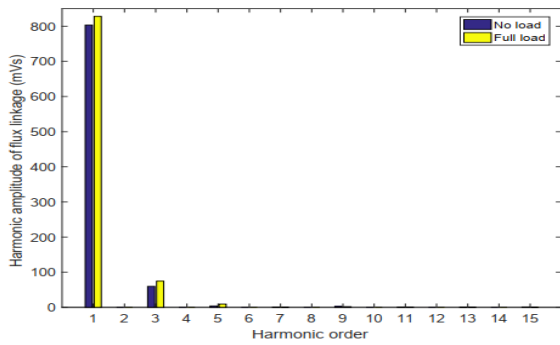


Figure 17. Harmonics order of the flux linkage under no load and full load mode

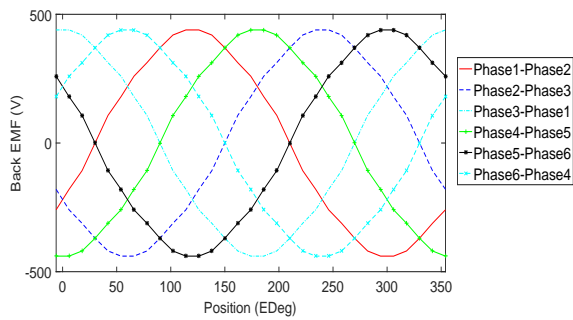


Figure 18. Back EMF waveform using the skewing technique

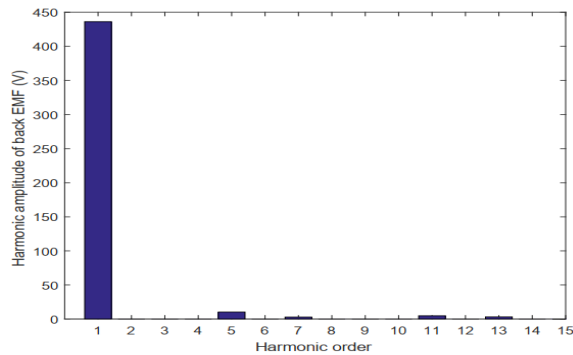


Figure 19. Harmonic components of the back EMF

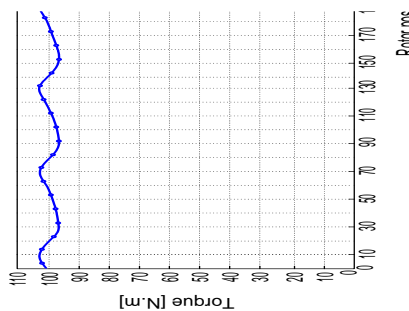


Figure 20. Output torque waveform

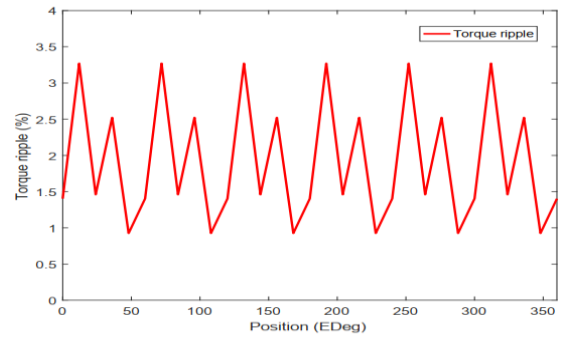


Figure 21. Torque ripple waveform

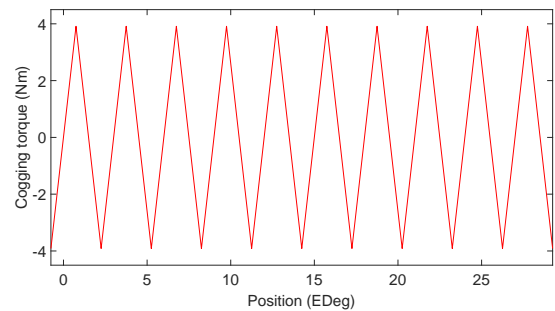


Figure 22. Cogging torque waveform

6. CONCLUSION

In this paper, the required parameters of the 7.5 kW six-phase outer rotor SPMSM using the PM material of NdFeB (N38) have been successfully obtained by the analytic model. The FEM has been also applied to verify and simulate the electromagnetic parameters of the proposed motor, such as the waveform of back EMF, output torque torque ripple and cogging torque by using the skewing PM technique. The magnetic flux density in air gap, harmonic components of the air gap flux density and waveform of flux linkage under no and full load operations have been also successfully presented. The obtained results can be served as useful reference for designers, researchers and manufactures to go on completing the prototype of design for the 7.5 kW six-phase outer rotor SPMSM. This is also a foundation for many subsequent studies, including potential research areas such as optimizing design calculations using optimization methods like genetic algorithms, swarm optimization, etc.

The developed method could be extended for calculating the network from equivalent resistances for each part of the motor. This process helps determine the waveforms of important parameters during the motor's operation, such as air gap flux density, dynamic reactance waveform, output torque waveform, as well as tooth torque waveform. Subsequently, various approaches can be proposed to improve the waveforms of these motor

parameters, aiming to enhance the overall optimization of the motor.

7. AUTHOR CONTRIBUTIONS

Authors Trinh Truong Cong and Vuong Dang Quoc conducted the research and simulation. Authors Thanh Nguyen Vu, Ha Vo Thanh and Dinh Bui Minh analyzed results. Author Vuong Dang Quoc wrote the paper; all authors had approved the final manuscript.

8. ACKNOWLEDGEMENT

This research is funded by Hanoi University of Science and Technology (HUST) under project number T2023-PC-043.

The authors also gratefully acknowledges Quy Nhon University, created favorable conditions for the authors to use the copyright-supported Ansys software program to compute and simulate the practical problem in this research. This software is the package belonging to ANSYS Electronics Desktop V19. R1.

9. REFERENCES

- Wei Y, Si J, Cheng Z, Xu S, Dong L, Liang J. Design and characteristic analysis of a six-phase direct-drive permanent magnet synchronous motor with 60° phase-belt toroidal winding configuration for electric vehicle. *IET Electric Power Applications*. 2020;14(13):2659-66. 10.1049/iet-epa.2020.0083
- Patel VI, Wang J, Wang W, Chen X. Six-phase fractional-slot-per-pole-per-phase permanent-magnet machines with low space harmonics for electric vehicle application. *IEEE Transactions on Industry Applications*. 2014;50(4):2554-63. 10.1109/TIA.2014.2301871
- Scuiller F, Semail E, Charpentier J-F, Letellier P. Multi-criteria-based design approach of multi-phase permanent magnet low-speed synchronous machines. *IET Electric Power Applications*. 2009;3(2):102-10. 110. 10.1049/iet-epa:20080003
- Islam MZ, Bonthu SSR, Choi S, editors. Comparison of two different winding topologies for external-rotor five-phase PM-assisted synchronous reluctance motor in vehicle applications. 2017 IEEE International Electric Machines and Drives Conference (IEMDC); 2017: IEEE. 10.1109/IEMDC.2017.8002399
- Jin F, Si J, Cheng Z, Su P, Dong L, Qi G, editors. Analysis of a six-phase direct-drive permanent magnet synchronous motor with novel toroidal windings. 2019 IEEE Vehicle Power and Propulsion Conference (VPPC); 2019: IEEE.
- Del Pizzo A, Di Noia LP, Di Tommaso AO, Miceli R, Rizzo R, editors. Comparison between 3-ph and 6-ph PMSM drives for the electric propulsion of unmanned aerial vehicles. 2021 IEEE 15th International Conference on Compatibility, Power Electronics and Power Engineering (CPE-POWERENG); 2021: IEEE. 10.1109/CPE-POWERENG50821.2021.9501082
- Won H, Hong Y-K, Platt J, Choi M, Bryant B, Choi S, editors. Six-phase fractional-slot concentrated winding ferrite spoke-type permanent magnet synchronous motor for electric truck. 2021 IEEE International Electric Machines & Drives Conference (IEMDC); 2021: IEEE.
- Iyer LV, Lai C, Dhulipati H, Mukundan S, Mukherjee K, Kar N. Investigation of a Six-Phase Interior Permanent Magnet Synchronous Machine for Integrated Charging and Propulsion in EVs. *SAE International Journal of Alternative Powertrains*. 2018;7(2):103-16.
- Cheng L, Sui Y, Zheng P, Yin Z, Wang C. Influence of stator MMF harmonics on the utilization of reluctance torque in six-phase PMA-SynRM with FSCW. *Energies*. 2018;11(1):108.
- Won H, Hong Y-K, Lee W, Choi M. Roles of coercivity and remanent flux density of permanent magnet in interior permanent magnet synchronous motor (IPMSM) performance for electric vehicle applications. *AIP Advances*. 2018;8(5).
- Zhu Z, Howe D. Influence of design parameters on cogging torque in permanent magnet machines. *IEEE Transactions on energy conversion*. 2000;15(4):407-12.
- Gao C, Gao M, Si J, Hu Y, Gan C. A novel direct-drive permanent magnet synchronous motor with toroidal windings. *Energies*. 2019;12(3):432.
- Heins G, Ionel DM, Thiele M. Winding factors and magnetic fields in permanent-magnet brushless machines with concentrated windings and modular stator cores. *IEEE Transactions on Industry Applications*. 2015;51(4):2924-32.
- Potgieter JH, Kamper MJ. Double PM-rotor, toothed, toroidal-winding wind generator: A comparison with conventional winding direct-drive PM wind generators over a wide power range. *IEEE Transactions on Industry Applications*. 2016;52(4):2881-91.
- Madhavan R, Fernandes BG. Axial flux segmented SRM with a higher number of rotor segments for electric vehicles. *IEEE Transactions on Energy Conversion*. 2013;28(1):203-13.
- Zhu L, Jiang S, Zhu Z, Chan C. Analytical methods for minimizing cogging torque in permanent-magnet machines. *IEEE transactions on magnetics*. 2009;45(4):2023-31.
- Won H, Hong Y-K, Choi M, Platt J, Bryant B, Choi S, et al. Novel design of six-phase spoke-type ferrite permanent magnet motor for electric truck application. *Energies*. 2022;15(6):1997. <https://doi.org/10.3390/en15061997>

COPYRIGHTS

©2024 The author(s). This is an open access article distributed under the terms of the Creative Commons Attribution (CC BY 4.0), which permits unrestricted use, distribution, and reproduction in any medium, as long as the original authors and source are cited. No permission is required from the authors or the publishers.

**Persian Abstract****چکیده**

موتورهای سنکرون آهنربای دائم چند فاز (PMSM) به دلیل گشتاور بالا، راندمان و عملکرد قابل اعتماد، در زمینه صنعت (مانند کامیون ها، نیروی محرکه کشتی، معدن و غیره) کاربرد زیادی دارد. تاکنون، بسیاری از محققان PMSM چند فاز (به عنوان مثال، PMSM سه فاز، PMSM شش فاز) را برای کاربردهای خودروهای الکتریکی مورد مطالعه قرار داده اند. اما، هنوز محدودیت های قابل توجهی در کمیت تحقیقات در مورد PMSM های شش فاز وجود دارد. به ویژه، هنگام تحقیق در مورد این نوع موتور، نویسندگان عمدتاً مشخصات PMSM های شش فاز را ارائه کرده و سپس آزمایشاتی را بر روی این ماشین ها بدون ارائه فرمول های دقیق برای محاسبه تحلیلی و طراحی ابعاد و پارامترهای الکترومغناطیسی انجام داده اند. در این تحقیق، ابتدا یک مدل تحلیلی برای تعیین پارامترهای اصلی یک PMSM شش فاز روی سطح (SPMSM) توسعه داده شد. سپس روش اجزای محدود (FEM) برای شبیه سازی و محاسبه پارامترهای الکترومغناطیسی، مانند شکل موج جریان، نیروی الکتروموتور برگشتی (EMF)، توزیع چگالی شار، گشتاور خروجی، گشتاور چرخشی، ریپل گشتاور و اجزای هارمونیک معرفی می شود. توسعه روش های پیشنهادی بر روی یک مشکل عملی SPMSM شش فاز ۷.۵ کیلووات اعمال می شود.